



HAL
open science

Probing the Menasemiquinone Binding Mode to Nitrate Reductase A by Selective 2 H and 15 N Labeling, HYSCORE Spectroscopy, and DFT Modeling

Maryam Seif eddine, Frédéric Biaso, Rodrigo Arias-cartin, Eric Pilet, Julia Rendon, Sevdalina Lyubenova, Farida Seduk, Bruno Guigliarelli, Axel Magalon, Stephane Grimaldi

► To cite this version:

Maryam Seif eddine, Frédéric Biaso, Rodrigo Arias-cartin, Eric Pilet, Julia Rendon, et al.. Probing the Menasemiquinone Binding Mode to Nitrate Reductase A by Selective 2 H and 15 N Labeling, HYSCORE Spectroscopy, and DFT Modeling. *ChemPhysChem*, 2017, 18 (19), pp.2704-2714. 10.1002/cphc.201700571 . hal-01635739

HAL Id: hal-01635739

<https://amu.hal.science/hal-01635739>

Submitted on 23 Apr 2018

HAL is a multi-disciplinary open access archive for the deposit and dissemination of scientific research documents, whether they are published or not. The documents may come from teaching and research institutions in France or abroad, or from public or private research centers.

L'archive ouverte pluridisciplinaire **HAL**, est destinée au dépôt et à la diffusion de documents scientifiques de niveau recherche, publiés ou non, émanant des établissements d'enseignement et de recherche français ou étrangers, des laboratoires publics ou privés.

Special
Issue

Probing the Menasemiquinone Binding Mode to Nitrate Reductase A by Selective ^2H and ^{15}N Labeling, HYSCORE Spectroscopy, and DFT Modeling

Maryam Seif Eddine,^[a] Frédéric Biaso,^[a] Rodrigo Arias-Cartin,^[b] Eric Pilet,^[a, c] Julia Rendon,^[a] Sevdalina Lyubenova,^[d] Farida Seduk,^[b] Bruno Guigliarelli,^[a] Axel Magalon,^[b] and Stéphane Grimaldi*^[a]

In vivo specific isotope labeling at the residue or substituent level is used to probe menasemiquinone (MSK) binding to the quinol oxidation site of respiratory nitrate reductase A (NarGHI) from *E. coli*. ^{15}N selective labeling of His $^{15}\text{N}\delta$ or Lys $^{15}\text{N}\zeta$ in combination with hyperfine sublevel correlation (HYSCORE) spectroscopy unambiguously identified His $^{15}\text{N}\delta$ as the direct hydrogen-bond donor to the radical. In contrast, an essentially anisotropic coupling to Lys $^{15}\text{N}\zeta$ consistent with a through-space magnetic interaction was resolved. This suggests that MSK does not form a hydrogen bond with the side chain of the nearby Lys86 residue. In addition, selective ^2H labeling of the menaquinone methyl ring substituent allows unambiguous

characterization of the ^2H —and hence of the ^1H —methyl isotropic hyperfine coupling by ^2H HYSCORE. DFT calculations show that a simple molecular model consisting of an imidazole N δ atom in a hydrogen-bond interaction with a MSK radical anion satisfactorily accounts for the available spectroscopic data. These results support our previously proposed one-sided binding model for MSK to NarGHI through a single short hydrogen bond to the N δ of His66, one of the distal heme axial ligands. This work establishes the basis for future investigations aimed at determining the functional relevance of this peculiar binding mode.

1. Introduction

Isoprenoid quinones are amphiphilic molecules found in nearly all living organisms in which they act as key players in bioenergetic processes.^[1] They are, for example, involved in the coupled electron/proton transfer reaction in bacterial and plant photosynthesis and in the energy transducing membrane proteins of mitochondrial or prokaryotic respiratory chains. Although all characterized isoprenoid quinones bear a ring moiety with two oxygen atoms at positions 1 and 4, their structure and redox properties can significantly differ. The great majority of biological isoprenoid quinones belong to the benzoquinones (e.g., ubiquinones or plastoquinones) or to the naphthoquinones types (e.g., phyloquinones or menaquinones (MK)).^[2] Among them, low redox potential menaqui-

nonones (or vitamins K₂) are the most widely distributed quinones in living organisms and most likely represent the ancestral quinones present in the Last Universal Common Ancestor of prokaryotes.^[2,3] The crucial role of isoprenoid quinones in bioenergetics relies mainly on two properties: (i) their soluble character in biological membrane lipid bilayers conferred by their apolar hydrophobic side chain that can vary in length, in the degree of saturation, and in the presence of additional groups; (ii) the redox properties of their aromatic ring, which can easily and reversibly oscillate in physiological conditions between three different oxidation states with different protonation levels: the oxidized deprotonated quinone state, the intermediate semiquinone (SQ) form, which can be anionic (SQ⁻) or neutral (SQH[•]), and the fully reduced and protonated quinol state.

Quinones interact with bioenergetic complexes within well-defined protein sites (called Q sites) where they transiently bind and exchange with the Q-pool, or act as a permanently bound cofactor, which is possibly involved in intramolecular electron transfer. Previous studies on photosynthetic and respiratory complexes have shown that the Q site properties can drastically modify the quinone chemical properties and therefore the Q site reactivity, hereby contributing to define the directionality of the electron transfer mechanism in a particular enzyme or its specificity towards quinones.^[4,5] Importantly, modulating these interactions allows to tune the stability and the lifetime of the highly reactive semiquinone intermediate,

[a] M. Seif Eddine, Dr. F. Biaso, Dr. E. Pilet, Dr. J. Rendon, Prof. B. Guigliarelli, Dr. S. Grimaldi
Aix Marseille University, CNRS, BIP, Marseille (France)
E-mail: grimaldi@imm.cnrs.fr

[b] Dr. R. Arias-Cartin, F. Seduk, Dr. A. Magalon
Aix Marseille University, CNRS, LCB, Marseille (France)

[c] Dr. E. Pilet
Faculté de Biologie, University Pierre et Marie Curie, Paris (France)

[d] Dr. S. Lyubenova
EPR Division, Bruker Biospin GmbH, Rheinstetten (Germany)

Supporting Information and the ORCID identification number(s) for the author(s) of this article can be found under:
<https://doi.org/10.1002/cphc.201700571>.

An invited contribution to a Special Issue on Physical Chemistry in France

which contributes to cellular oxidative stress owing to its high reactivity towards dioxygen.^[6–8] A crucial parameter for these interactions is the formation of hydrogen bonds between the quinone oxygens and surrounding amino acid residues. Understanding the factors that finely tune the Q site reactivity requires obtaining high-resolution information on protein–quinone interactions. This is a challenging task because of the size and the membranous nature of the bioenergetic complexes, but also because of the transient character of the interactions and the complex chemistry that occurs in Q sites. Hence, only a few high-resolution crystal structures of these complexes with bound quinones are available and the characterization of structural modifications occurring in the Q site during enzyme turnover remains challenging.^[9]

In this context, spectroscopic techniques such as electron paramagnetic resonance (EPR) and in particular hyperfine spectroscopies for example, electron nuclear double resonance (ENDOR), electron spin echo envelope modulation (ESEEM) spectroscopy, and its two-dimensional variant hyperfine sublevel correlation (HYSCORE) spectroscopy are powerful in providing high-resolution structural data on SQ intermediates in bioenergetic complexes.^[5,10,11] They allow the detection of magnetic nuclei (e.g., naturally abundant ¹H and ¹⁴N) located in the immediate vicinity of the radical such as those belonging to the quinone itself, to the solvent, or to nearby amino acids. Assigning the detected ¹H and ¹⁴N nuclei to a particular chemical group is not straightforward. For this purpose, various strategies have been used, including (i) uniform enrichment of the protein in ²H^[12–14] or ¹⁵N^[15–22] or of the solvent thanks to H₂O/²H₂O exchange experiments;^[12,23–28] (ii) theoretical calculations of hyperfine and quadrupolar parameters,^[13,29–33] (iii) reconstitution experiments using exogenous quinones with various substituents or chemically labeled with ²H,^[29,34] and (iv) comparison with spectroscopic data obtained on model SQs measured in organic solvents.^[35–39] A direct and more physiological strategy relies on in vivo isotope labeling of individual amino acids or sets of amino acids, which, however, requires engineered auxotrophic strains supplemented with isotopically enriched amino acids.^[40–42] With this strategy, selectively ¹⁵N-labeled cyt *bo*₃ samples from *E. coli* were used in ¹⁵N HYSCORE experiments to identify the amino acids interacting with the stabilized ubisemiquinone species bound at the high affinity quinone binding site (Q_H) of the wild-type enzyme or in a Q-site mutant.^[43,44] A reverse labeling approach in which this enzyme was uniformly ¹⁵N-labeled except for selected amino acid types has also been used.^[44]

In this work, ²H and ¹⁵N in vivo selective labeling is used to resolve quinone–protein interactions in the respiratory nitrate reductase (Nar) from *E. coli*, a widely distributed prokaryotic enzyme that allows anaerobic respiration with nitrate as a terminal electron acceptor. This membrane-bound heterotrimeric complex (NarGHI) couples the oxidation of membrane quinols at a periplasmically oriented Q site to the cytoplasmic two-electron reduction of nitrate into nitrite.^[47,48] NarGHI turnover induces a net translocation of protons across the membrane, which contributes to maintaining the transmembrane proton gradient that drives, for instance, ATP synthesis. The NarG cata-

lytic subunit holds the Mo-bis-pyranopterin guanosine dinucleotide cofactor and a FeS cluster.^[49] The electron transfer subunit NarH harbors four FeS clusters. Finally, the cytoplasmically exposed NarGH subunits are connected to the membrane-integral NarI, which has two *b*-type hemes termed *b*_D and *b*_P according to their respective distal and proximal positions with respect to the nitrate reducing site.^[48] The metal cofactors form a chain of electron transfer relays from the quinol oxidation site Q_D in NarI to the molybdenum atom.

By combining site directed mutagenesis experiments, redox potentiometry, and EPR techniques, we have demonstrated that *E. coli* NarGHI stabilizes in the Q_D site the semiquinone form of the three respiratory quinones available in this organism, namely menaquinone (MSK), ubisemiquinone (USQ), and demethylmenaquinone (DMSK).^[18,46,50,51] Moreover, their radical intermediates exhibit a similar interaction with a single ¹⁴N nucleus in their ¹⁴N HYSCORE spectra. The nuclear quadrupole parameters (κ , η) were accurately determined by 3 GHz ESEEM/HYSCORE experiments for the MSK at the Q_D site (hereafter referred to as MSK_D), leading to (κ , η) = (0.49 MHz, 0.5). We previously assigned this nitrogen to the heme *b*_D axial ligand His66 based on the following observations: (i) these (κ , η) values are very close to those measured for N δ histidine nitrogens, that is, (κ , η) = (0.35–0.41 MHz, 0.61–0.82) according to literature data,^[10,11] (ii) although no crystal structure of the enzyme has been solved with a bound quinone, a structure of NarGHI in complex with an inhibitor, pentachlorophenol (PCP), is available, with its hydroxyl group involved in a hydrogen bond with His66 N δ ,^[45] (iii) site-directed mutagenesis experiments indicate that no MSK is stabilized in NarGHI mutants lacking heme *b*_D or when Lys86, a residue located in the Q_D site (Figure 1 A), is substituted into Ala,^[46,50] and (iv) no His residue other than His66 is present in the NarGHI Q_D site. However, direct evidence for the attribution of this nitrogen is still lacking and the role of Lys86 remains to be elucidated.

Interestingly enough, high-resolution EPR studies performed on MSK_D in combination with H₂O/²H₂O exchange experiments resolved hyperfine interactions with two nonexchangeable protons (H1 and H2) that likely correspond to methyl and methylene protons.^[23] Corresponding hyperfine couplings were estimated from contour line shape analysis of ¹H HYSCORE spectra. This led to two possible solutions for the H1 isotropic hyperfine coupling constant [$|A_{\text{iso}}|(\text{H1}) = 6.8$ or 5.5 MHz]. Based on its characteristics, that is, a predominant isotropic hyperfine coupling and a weak hyperfine anisotropy that is comparable to that found in the literature for methyl protons,^[10] this coupling was attributed to the three equivalent methyl protons substituting the MK aromatic ring. Accordingly, the preferred hyperfine set for these protons was (A_{iso} , T)(H1) = (± 5.5 , ± 1.25) MHz. However, this unusually small isotropic value reflects a singularly low spin density on the quinone carbon α carrying the methyl group. This was ascribed to strong asymmetry of the MSK_D binding mode, leading to a low spin density on the carbon *ortho* to the hydrogen-bonded oxygen. In addition, H2 with (A_{iso} , T) = (± 1.0 , ± 1.2) MHz was tentatively assigned to one of the β -methylene isoprenyl protons. Moreover, a single exchangeable proton coupling (H3)

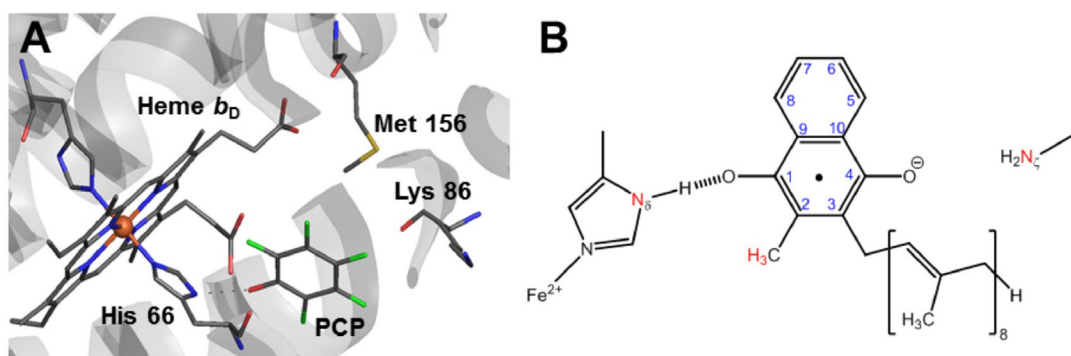


Figure 1. A) Detailed view of the NarGHI PCP binding site (PDB entry: 1Y4Z).^[45] The b_D heme, PCP, and side chains of residues forming the Q_D site and discussed in this work are shown in stick rendering. B) Working model of MSK_b binding based on our previous spectroscopic work.^[18,23,46] Strongly asymmetric binding of the radical occurs through a short in-plane hydrogen bond to the His66 N_δ , whereas Lys86 does not appear to be a direct hydrogen-bond donor to the intermediate. The MSK_b O4 oxygen is deprotonated. Surrounding nuclei selectively enriched in ^{15}N or ^2H in this work are colored in red. The numbering of carbon atoms in the menaquinone ring is also indicated.

was detected by ^1H HYSCORE or Q-band ^2H pulsed ENDOR. Based on (i) its almost zero isotropic contribution [$A_{\text{iso}}(\text{H3}) \approx 0.06$ MHz] (ii) its large anisotropy [$T(\text{H3}) \approx 5.7$ MHz], and (iii) on the quadrupole coupling constant of the corresponding exchanged deuteron [$\kappa(^2\text{H3}) \approx 0.18$ MHz], it was assigned to a proton involved in a short (≈ 1.6 Å) in-plane hydrogen bond between the O1 oxygen and the N_δ of the interacting His residue. Altogether, these results were interpreted by a model involving single-sided hydrogen bonding to the quinone oxygen O1, according to the atom numbering shown in Figure 1 B.

In this work, to overcome the existing uncertainties concerning the MSK_b binding mode, we employed two selective labeling strategies: (i) we directly identified the hydrogen-bonded nitrogen atom and probed the role of the nearby Lys86 residue in the MSK_b binding mode by using ^{15}N selective labeling of NarGHI on His with ^{15}N on N_δ or on Lys with ^{15}N on N_ζ , (ii) we unambiguously identified the isotropic hyperfine characteristics of the MSK_b methyl protons by employing ^2H selective labeling of the methyl substituent of menaquinone and direct detection of ^2H hyperfine coupling by HYSCORE. Eventually, based on the available structural data and DFT calculations, we provide a simple molecular model that satisfactorily accounts for the available $^{14,15}\text{N}$ and $^{1,2}\text{H}$ hyperfine data on MSK_b . Our results support an extreme asymmetry of the MSK_b binding mode.

2. Results and Discussion

2.1. ^{15}N HYSCORE Spectroscopy on NarGHI-bound MSK_b from Histidine or Lysine Auxotrophic *E. coli* Strains

The X-band ^{14}N HYSCORE spectrum of MSK_b shown in Figure 2A was previously described in detail.^[18,50,51] It exhibits two cross peaks (1 in Figure 2A) correlating nuclear transition frequencies at 2.2 and 3.4 MHz from opposite electron spin manifolds. These were assigned to the two double-quantum transition frequencies from a weakly coupled ^{14}N nucleus with $A_{\text{iso}}(^{14}\text{N}) \approx 0.8$ MHz. This nitrogen produces cross peaks 2 in the HYSCORE spectrum of MSK_b measured on uniformly ^{15}N en-

riched NarGHI (Figure 2B). They have maxima at 1.0 MHz and 2.0 MHz and are centered symmetrically with respect to the ^{15}N Larmor frequency ($\nu_L(^{15}\text{N}) \approx 1.5$ MHz). An additional prominent peak 3 is detected on the diagonal at $\nu_L(^{15}\text{N})$. It is contributed by ^{15}N nuclei around MSK_b that are involved in weak interactions with the unpaired electron. Owing to the influence of the nuclear quadrupole interaction, no corresponding peak is detected near $\nu_L(^{14}\text{N})$ in the ^{14}N HYSCORE spectrum shown in Figure 2A.^[16,17,19,43] To directly identify the origin of these signals, we constructed histidine and lysine auxotrophs from the *E. coli* JCB4023 strain. Inner membrane vesicles containing overproduced NarGHI were purified and titrated to generate MSK_b in equilibrium conditions. The X-band continuous-wave (cw) EPR spectra of these radicals were identical to those measured for MSK_b in unlabeled or in uniformly ^{15}N -labeled NarGHI (not shown).^[18] These radicals were further studied by HYSCORE spectroscopy. Figure 2C shows the spectrum of MSK_b in NarGHI with ^{15}N -labeled His N_δ . It exhibits a single pair of cross features correlating frequencies 1.0 MHz and 2.0 MHz, corresponding to cross peaks 2. This demonstrates unambiguously that both are produced by an interaction with a His N_δ nucleus, in line with our previous assignment of this nucleus to the N_δ of the heme b_D axial ligand His66. The absence of a diagonal peak at $\nu_L(^{15}\text{N})$ in the spectrum shown in Figure 2C is consistent with available X-ray data. Indeed, inspection of the NarGHI crystal structures predicts that, apart from His66, the closest His residue to MSK_b is the other heme b_D axial ligand, His187, which is situated too far from the radical [$r_{\text{PCP01-His187N}_\delta} \approx 9.8$ Å] to contribute to the HYSCORE spectrum shown in Figure 2C. Figure 2D shows the spectrum of MSK_b in NarGHI with ^{15}N -labeled N_ζ in Lys. In addition to the unchanged ^{14}N features 1 and in contrast to the spectrum shown in Figure 1 C, it resolves a diagonal peak 3' at $\nu_L(^{15}\text{N})$ assigned to weakly coupled Lys $^{15}\text{N}_\zeta$. The homogeneous shape of this peak indicates a negligible isotropic hyperfine coupling constant and its width is well simulated by assuming an isotropic hyperfine interaction with $A_{\text{iso}}(^{15}\text{N}) < 0.1$ MHz. Hence, this nucleus does not appear to carry any significant electron spin density. This is consistent with a through-space interaction between the un-

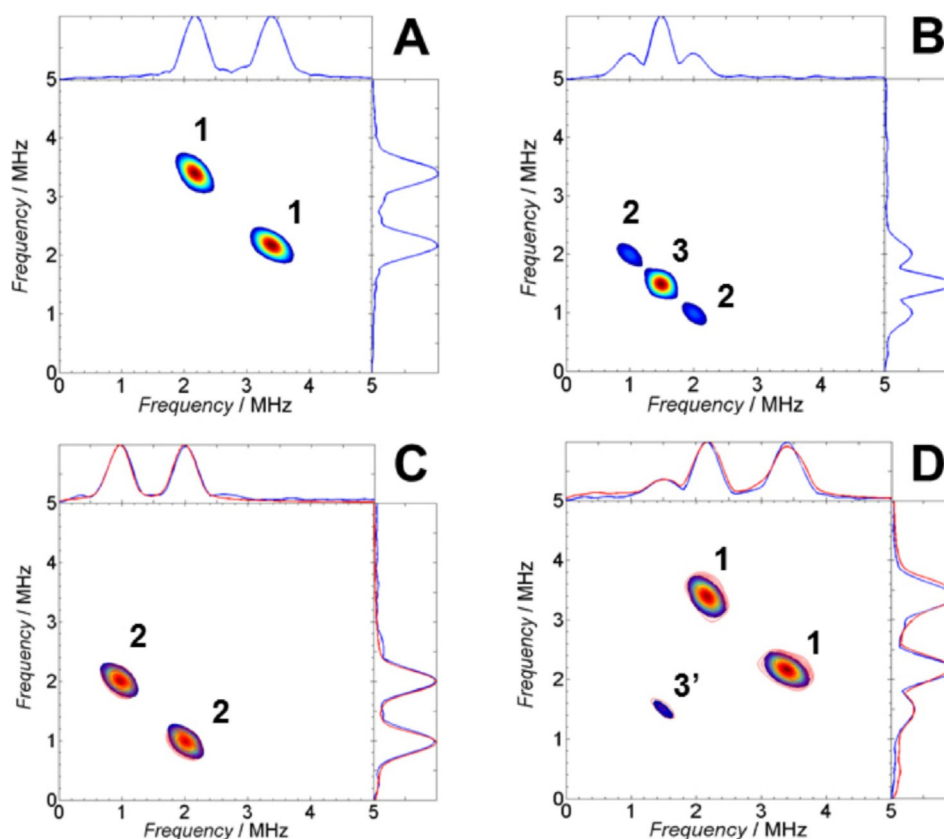


Figure 2. Contour presentations of the low-frequency part of representative HYSCORE spectra of MSK_D by using either unenriched NarGHI (A), uniform ^{15}N enrichment of NarGHI (B), selectively ^{15}N -labeled NarGHI on His N δ (C), or selectively ^{15}N -labeled NarGHI on Lys N ζ (D). Experimental conditions: time between first and second pulses τ , 136 ns (A) or 204 ns (B, C, D); $\pi/2$ pulse length, 12 ns; π pulse length, 24 ns (A) or 12 ns with optimized amplitude (B, C, D); microwave frequency, 9.6967 GHz (A), 9.6900 GHz (B), 9.6812 GHz (C), 9.6794 GHz (D); magnetic field, 345.3 mT (A), 345.1 mT (B), 345.0 mT (C), 344.8 mT (D); sample redox potential and pH value, -141 mV, pH 8.5 (A), -104 mV, pH 7.5 (B), -147 mV, pH 8.5 (C), -139 mV, pH 8.5 (D). Simulations are shown as red contour plots superimposed to the experimental spectrum. The spectrum (D) was simulated by considering two independent spin systems, each with a single magnetically coupled nitrogen nucleus.^[19] Simulation parameters and their estimated errors are: (C) $(A_{\text{iso}}, T)(^{15}\text{N}) = (0.97 \pm 0.02, 0.30 \pm 0.02)$ MHz; (D) $(A_{\text{iso}}, T)(^{15}\text{N}) = (0 \pm 0.1, 0.45 \pm 0.10)$ MHz; $(A_{\text{iso}}, T)(^{14}\text{N}) = (0.70 \pm 0.04, 0.20 \pm 0.02)$ MHz; quadrupole parameters $(\kappa, \eta)(^{14}\text{N}) = (0.42 \pm 0.07 \text{ MHz}, 0.50 \pm 0.05)$ with Euler angles $(0^\circ, 120^\circ, 30^\circ)$ to the g -frame.

paired electron of MSK_D and this nucleus, in agreement with our previous experiments detecting a single exchangeable proton magnetically coupled to MSK_D . Given that Lys86 is the only Lys residue within the Q_D site, peak 3' is assigned to Lys86 N ζ . These spectroscopic results are therefore qualitatively consistent with the NarGHI crystal structure with bound PCP (PDB entry: 1Y4Z), which shows a long distance between the PCP C14 atom and Lys86 N ζ $r_{\text{PCP C14-Lys86 N}\zeta} = 5.9 \text{ \AA}$. Notably, the high B-factor found at this position might reflect a functionally relevant high mobility of this residue. As previously suggested, a movement of the Lys86 side chain could occur during the quinol oxidation mechanism and could be associated to protonation/deprotonation events taking place during enzyme turnover, allowing protons to be released to the periplasm.^[18,45] Overall, these results support our previously proposed model of a strongly asymmetric binding mode of MSK_D through a single hydrogen bond to His66 N δ .^[23]

2.2. ^2H HYSCORE Spectroscopy on NarGHI-bound MSK from Methionine Auxotrophic *E. coli* Strain

To directly measure the hyperfine coupling to the methyl protons of MSK_D , NarGHI was overproduced in a methionine auxotroph *E. coli* strain grown in a minimal medium supplemented with ^2H -labeled L-methionine at the side chain methyl group. Indeed, the menaquinone methyl group originates from S-adenosylmethionine in the menaquinone biosynthetic pathway. A similar biosynthetic deuteration strategy of phyloquinones in the cyanobacterium *Anabaena variabilis* allowed the identification of hyperfine coupling to the methyl protons of the photosystem 1 secondary electron acceptor $A_1^{* -}$ by using ^1H ENDOR.^[42] In addition, a similar approach using selectively ^{13}C -labeled methionines allowed selective ^{13}C enrichment of the methyl and methoxy substituents of ubisemiquinone bound at the cyt bo_3 Q_H site from *E. coli* or at the bc_1 complex Q_i site from *Rhodobacter sphaeroides*.^[52,53] NarGHI-enriched inner membrane vesicles were purified from the methionine-deficient strain mentioned above, titrated, and studied by EPR spectroscopy. The cw EPR spectrum of a sample poised at

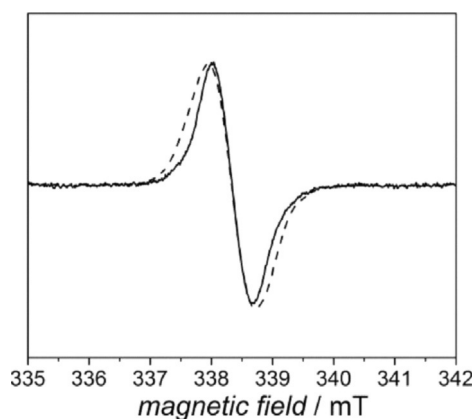


Figure 3. EPR spectra of menaemiquinone radicals without (dashed trace) or with ^2H -labeled methyl group (solid trace) stabilized in NarGHI-enriched membranes from *E. coli*. Experimental conditions: sample redox potential, -156 mV and -158 mV for MSK and C^2H_3 -MSK, respectively; sample pH, 8.5; temperature, 60 K; microwave power, 0.1 mW; field modulation amplitude, 0.3 mT at 100 kHz; microwave frequencies, 9.4804 GHz and 9.4089 GHz for C^2H_3 - or unlabeled MSK_D , respectively. Magnetic fields have been corrected with respect to an offset against a weak pitch sample.

-158 mV is shown in Figure 3. It shows an intense unstructured isotropic radical signal centered at $g_{\text{av}} \approx 2.0045$ with a peak-to-peak line width of about 0.6 mT assigned to NarGHI-bound MSK_D with a ^2H -labeled methyl group, hereafter referred to as C^2H_3 - MSK_D . The EPR peak-to-peak line width of C^2H_3 - MSK_D decreases by ≈ 0.2 mT with respect to that measured for unlabeled MSK_D (Figure 3, dashed trace), indicating a significant contribution of the methyl protons hyperfine coupling to the MSK_D EPR linewidth. To increase the spectral resolution and detect the ^2H hyperfine couplings, this sample was further investigated by HYSOCORE spectroscopy.

The (+, +) quadrant of a representative HYSOCORE spectrum measured with the time, τ , between the first and second pulses of 204 ns is shown in Figure 4 in the 0 to 5 MHz frequency interval. In addition to the ^{14}N cross peaks 1 discussed

above and in our previous works,^[18,50] ^2H lines are detected. They consist of a peak 4 located on the diagonal point ($\nu_{2\text{H}}$, $\nu_{2\text{H}}$) where $\nu_{2\text{H}}$ is the ^2H Larmor frequency, ≈ 2.3 MHz in the applied magnetic field. Moreover, a pair of well-resolved sharp cross peaks 5 with a circular shape is detected along the anti-diagonal, symmetrically around ($\nu_{2\text{H}}$, $\nu_{2\text{H}}$). It correlates frequencies 1.8 and 2.7 MHz. These peaks are assigned to the single quantum frequencies from ^2H nuclei of the ^2H -labeled MSK methyl substituent. Indeed, single quantum transitions of $l=1$ nuclei with weak nuclear quadrupole interactions are well resolved in contrast to the double quantum transitions that have very low intensity and are therefore not detected. Hence, a correlation pattern similar to that given by nuclei with $l=1/2$ is expected. It corresponds in the weak coupling regime (i.e., $A_{\text{iso}} < 2\nu_l$) to a pair of cross peaks symmetrically positioned with respect to the Larmor frequency ν_l of the interacting nucleus. Whereas the circular shape of the ^2H cross peaks indicates a predominantly isotropic hyperfine coupling with weak quadrupole coupling, a value $A_{\text{iso}}(^2\text{H}) \approx 0.9$ MHz can be estimated from the difference between the two correlated frequencies. Spectral simulations have been carried out to more accurately estimate the parameters, which account for the position and the width of the ^2H cross peaks. As expected, their position is very sensitive to the A_{iso} value, which is refined by using spectral simulations to $A_{\text{iso}}(^2\text{H}) = 0.85 \pm 0.05$ MHz. Scaled to ^1H , it corresponds to $A_{\text{iso}}(^1\text{H}) \approx 5.5 \pm 0.3$ MHz. This value is in full agreement with the $A_{\text{iso}}(^1\text{H}) \approx 5.5$ MHz of the strongest coupling to the nonexchangeable proton H1 determined from analysis of ^1H HYSOCORE spectra of MSK_D .^[23] These results therefore allow direct assignment of H1 to the three equivalent methyl protons of MSK_D .

The simulated linewidth of cross peaks 5 slightly exceeds the experimental one (Figure 4B). However, a systematic and independent variation of either $T(^2\text{H})$ (Figure S1 in the Supporting Information) or $\kappa(^2\text{H})$ (Figure S2) indicated that these two parameters differently affect the shape of the ^2H cross peaks, therefore allowing us to estimate an upper limit value for each

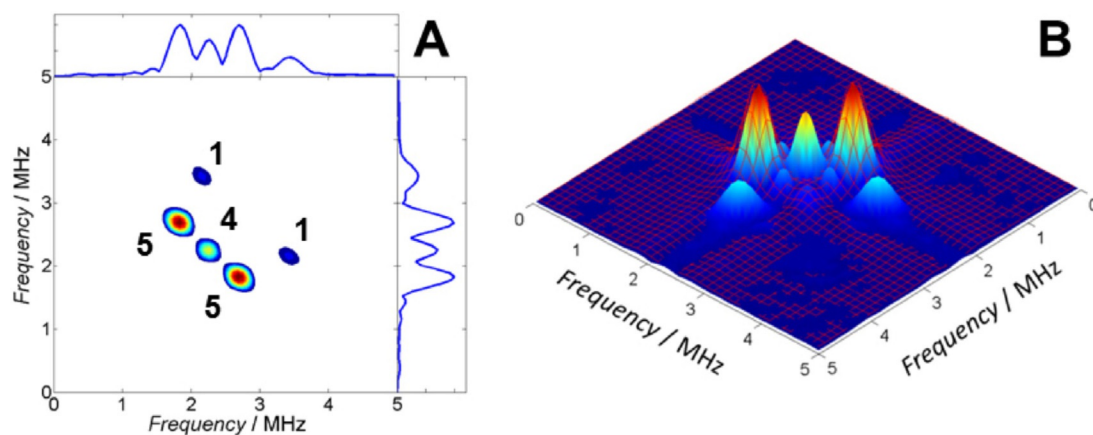


Figure 4. Contour (A) and stacked (B) presentations of the low-frequency part of the HYSOCORE spectrum of MSK_D with ^2H -labeled methyl group. Experimental conditions: magnetic field, 345.2 mT; time between first and second pulses, τ , 204 ns, microwave frequency, 9.6914 GHz, magnetic field, 345.2 mT. A simulation is shown as a red stacked plot superimposed to the experimental spectrum in panel B. Simulation parameters are: hyperfine parameters (A_{iso}, T) = (0.85, 0.2) MHz; quadrupole parameters (κ, η) = (0.05 MHz, 0), Euler angles were set to 0° .

of them. Hence, an upper limit for the anisotropic hyperfine coupling of $T(^2\text{H}) \approx 0.3$ MHz can be estimated, corresponding to $T(^1\text{H}) < 2$ MHz. Again, this value is consistent with our previous analysis of ^1H HYSCORE spectra of NarGHI-bound MSK_D , which led to $T(^1\text{H}) \approx 1.25$ MHz for H1. In addition, spectral simulations indicate that the quadrupole coupling constant of the methyl deuterons must satisfy $|\kappa| < 0.1$ MHz to produce the observed cross features (Figure S2) whereas η has no detectable influence.

The homogeneous shape of diagonal peak 4 at the ^2H Zeeman frequency indicates the presence of weak dipolar interactions between the unpaired electron and additional more distant ^2H nuclei. These ^2H most likely couple to MSK_D by a through-space dipolar interaction. An upper value of $T \approx 0.1$ – 0.2 MHz was estimated from simulations of the width of the central peak. Based on the DFT estimation of the spin density on the MSK O4 oxygen (section 2.3) of 0.22 and on Equation (1), a minimal distance of ≈ 3 – 3.8 Å between this methyl deuteron and the MSK_D O4 can be estimated. On the basis of the NarGHI crystal structure with bound PCP, we assigned this peak to the Met156 terminal CH_3 group whose C ϵ is located at ≈ 3.6 Å from the C14 atom of the PCP. Its side chain points toward the PCP in the Q_D site and could be involved in fine tuning the reactivity of the site toward quinones. This hypothesis is currently being assessed by site-directed mutagenesis in our laboratories. Other methionine residues are present in the Q_D site but are too far to contribute to the detected HYSCORE signal [$r_{\text{PCP}01\text{-Met}70\text{CH}_3} = 6.5$ Å, $r_{\text{PCP}14\text{-Met}89\text{CH}_3} = 7.0$ Å].

2.3. DFT Study

DFT calculations were performed on SQ models to obtain a structural model that accounts for the EPR spectroscopic data on MSK_D . The influence of hydrogen bonding on the SQ electronic structure has been extensively studied^[13, 14, 15, 29–31, 33, 35, 36, 54–59] and this work serves as a basis for the present study, which focuses on g -values as well as on ^1H hyperfine couplings, ^2H and ^{14}N nuclear quadrupole couplings. In the absence of a crystal structure of the NarI subunit with bound quinone, the starting chemical model we used in this study is based on our previously proposed working model and consists of a deprotonated MSK hydrogen bonded to the N δ of an imidazole ring (Figure 1B).^[23] This model is referred to as

Im- MSK hereafter. The Lys86 and Met156 residues are not considered here as they are too far to significantly influence the MSK_D electronic structure.

Systematic dependencies of the spectroscopic parameters on the geometry of the hydrogen bond have been investigated. Thus, four structural parameters were considered for geometry optimizations: the O1–H distance r_{OH} , the in-plane hydrogen bond angle α , the out-of-plane hydrogen bond angle β , and the twist angle φ between SQ and imidazole rings (Figure 5). Four series of calculations, one for each structural parameter, were performed. In each series, a single parameter among r_{OH} , α , β , or φ was set to a range of specific values while the three other parameters were kept constant. The isoprenoid chain of the SQ was truncated after the fourth carbon atom and oriented perpendicular to the quinone plane to minimize steric interactions with O4 and the methyl group.^[60, 61]

The range of explored α , β , and φ values was limited by steric constraints induced by replacing the PCP molecule in the corresponding NarGHI crystal structure (PDB entry: 1Y4Z) by a menaquinone, assuming that negligible rearrangements of neighboring residues occur. The α and β angles were investigated in the 0° – 30° range whereas the twist angle φ was constrained between 0° and 45° . The hydrogen bond length r_{OH} was varied between 1.60 and 1.90 Å. This range includes the value $r_{\text{OH}} = 1.62 \pm 0.02$ Å, which we evaluated from the measurement of the ^2H nuclear quadrupole coupling constant of the hydrogen-bonded deuteron to MSK_D .^[23] Eventually, a symmetric hydrogen-bonded MSK model was also tested as a reference, in which the SQ forms four hydrogen bonds with four 2-propanol molecules, as expected for a free menaquinone in alcoholic solution.^[39] For this model, hereafter referred to as $\text{IP}_4\text{-MSK}$, only the orientation of the isoprenoid chain was fixed, here perpendicular to the quinone plane, during geometry optimization.

Experimental g -values for MSK_D and MSK in 2-propanol are reported in Table 1. They are compared with those calculated by using a representative Im- MSK model (model 6, as defined in Table 2) or the $\text{IP}_4\text{-MSK}$ model. The calculated g -values are in remarkably good agreement with the experimental ones, as their difference does not exceed 3×10^{-4} . In addition, the experimentally observed increase of the g -tensor anisotropy of MSK_D with respect to the situation in alcoholic solvent is reasonably well reproduced in our models. In agreement with

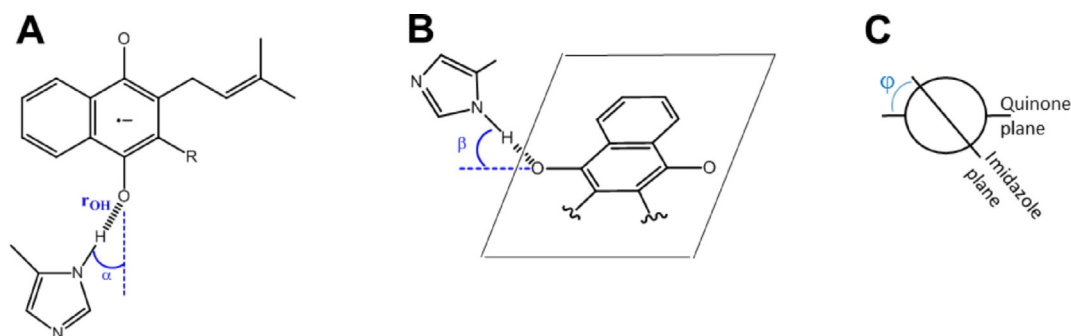


Figure 5. Definition of geometrical parameters investigated by using DFT calculations for the Im- MSK model. (A) Hydrogen-bond length r_{OH} and in-plane hydrogen-bond angle α ; (B) out-of-plane hydrogen-bond angle β ; (C) twist angle φ between the quinone and imidazole planes.

Table 1. Experimental and calculated g -values for MSK radical anions in different environments. All experimental values are determined from simulations of Q-band EPR spectra. Numbers in parentheses are the errors in the last digit.

	g_x	g_y	g_z	$g_x - g_z$	Reference
MSK _D	2.0061(1)	2.0051(1)	2.0023(1)	0.0038	[63]
Im-MSK model 6	2.00645	2.00516	2.00224	0.00424	this work
MSK in 2-propanol	2.00579(5)	2.00532(5)	2.00218(5)	0.00361	[39]
IP ₄ -MSK model	2.00584	2.00511	2.00221	0.00363	this work

Table 2. Geometrical parameters of Im-MSK models 1–6.

Models	r_{OH} [Å]	α [°]	β [°]	φ [°]
1	1.70	0	0	0
2	1.90	0	0	0
3	1.70	30	0	0
4	1.70	0	30	0
5	1.70	0	0	45
6	1.70	0	30	30

previous studies,^[30,56] the SQ g_x value was found to be the most sensitive to the investigated geometrical variations. However, in all tested Im-MSK models, the g_x value remained within the range 2.0063–2.0065. This is not surprising, as the g -tensor characteristics reflect the overall properties of the singly occupied molecular orbital (SOMO). Therefore, to investigate the MSK_D binding mode in greater detail, we rely next on the calculated hyperfine and quadrupolar parameters of selected nuclei that correspond to those in the vicinity of MSK_D, which are experimentally well characterized, that is, the His66 ¹⁴N δ , the single exchangeable ¹H and the MSK_D methyl ¹H.

Six representative Im-MSK models are selected that correspond to the geometrical parameters listed in Table 2, whereas the corresponding DFT-calculated hyperfine and quadrupolar parameters are reported in Table 3.

For the imidazole ¹⁴N δ nucleus, the most influential parameters are the hydrogen-bond length r_{OH} and the in-plane angle

α . In particular, the nuclear quadrupole coupling is strongly affected by these two parameters (Figure S3A,B). This tendency was already reported by Fritscher and co-workers.^[58]

One can notice that the out-of-plane angle has also a significant effect on the ¹⁴N hyperfine coupling constant (compare models 1 and 4). Similar conclusions can be drawn for the ¹H/²H hyperfine and quadrupolar couplings of the exchangeable hydrogen H_{exch} (Figure S3C,D). From these results, a good set of values is obtained for $r=1.70$ Å, $\alpha=0^\circ$, and $\beta=30^\circ$, that is, model 6. The twist angle φ has no significant influence on the calculated EPR parameters in the range of values investigated therein. Therefore, the value of $\varphi=30^\circ$ (model 6) has been arbitrarily chosen within the range of the possible values inferred from inspection of the NargHI X-ray structure with bound PCP. Regarding the MSK methyl group, ¹H/²H hyperfine and quadrupolar couplings are slightly affected by the modification of the four hydrogen-bond parameters. For all asymmetric models 1–6, the calculated $A_{\text{iso}}(^1\text{H}_{\text{Me}})$ lies between 5 and 6.3 MHz (Figure S3E,F), which is in excellent agreement with the experimental value $A_{\text{iso}}(^1\text{H}_{\text{Me}}) \approx 5.5$ MHz.^[23] The latter value is the smallest ever reported for methyl protons of vitamin K molecules bound to proteins or dissolved in protic solvents.^[16,29,34,35,39,42,63,64]

For the symmetric IP₄-MSK model, the calculated $A_{\text{iso}}(^1\text{H}_{\text{Me}}) \approx 7.5$ MHz is very similar to the experimental value $A_{\text{iso}}(^1\text{H}_{\text{Me}}) \approx 7.8$ MHz determined from X-band cw ENDOR spectra of MK₄^{•−} (4 refers to the number of isoprenoid units of the mena-semiquinone radical anion) in 2-isopropanol.^[39] The $A_{\text{iso}}(^1\text{H}_{\text{Me}})$ value is directly proportional to the unpaired spin density in the SQ π orbital on the adjacent α -carbon. Therefore, the large decrease between the value measured for MSK_D compared with that for MSK₄^{•−} must originate from the strong asymmetry of the spin density distribution in MSK_D. This is illustrated in Figure 6, which compares the Mulliken spin populations on the ring carbon and oxygen atoms in the Im-MSK model and in the IP₄-MSK model. It can be seen that the stronger hydrogen

Table 3. Experimental and calculated EPR parameters for Im-MSK models 1–6. n.d.: not determined. Experimental values are from [18,23].

Models	His66 N δ		H _{exch}		H _{Me}	
	$A_{\text{iso}}(^{14}\text{N})$ A_{tot} [MHz]	κ [MHz] η	$A_{\text{iso}}(^1\text{H})$ A_{tot} [MHz]	κ [MHz] η	$A_{\text{iso}}(^1\text{H})$ A_{tot} [MHz]	κ [MHz] η
exp	0.80 0.69; 0.69; 1.02	1.96 0.5	0.06 −5.67; −5.67; 11.52	0.18 0.2	5.53 4.28; 4.28; 8.03	< 0.1 n.d.
1	−0.53 −0.45; −0.56; −0.58	−1.97 0.60	0.30 −2.47; −3.41; 6.77	0.19 0.17	5.75 4.15; 4.89; 8.22	−0.06 0.01
2	−0.33 −0.25; −0.37; −0.38	−2.21 0.36	0.27 −2.02; −2.55; 5.38	0.21 0.16	6.25 4.62; 5.38; 8.75	−0.06 0.01
3	−0.31 −0.22; −0.35; −0.35	−2.27 0.36	0.19 −1.98; −2.25; 4.80	0.21 0.17	5.96 4.35; 5.08; 8.45	−0.06 0.02
4	1.08 0.89; 0.91; 1.43	−1.95 0.63	−0.33 −4.43; −4.90; 8.35	0.18 0.17	4.98 3.38; 4.14; 7.43	−0.06 0.01
5	−0.54 −0.46; −0.57; −0.59	−1.96 0.61	0.30 −2.42; −3.43; 6.75	0.19 0.17	5.66 4.06; 4.80; 8.12	−0.06 0.01
6	1.20 1.00; 1.03; 1.57	−1.95 0.62	−0.33 −4.50; −4.94; 8.46	0.18 0.17	5.07 3.46; 4.23; 7.53	−0.06 0.01

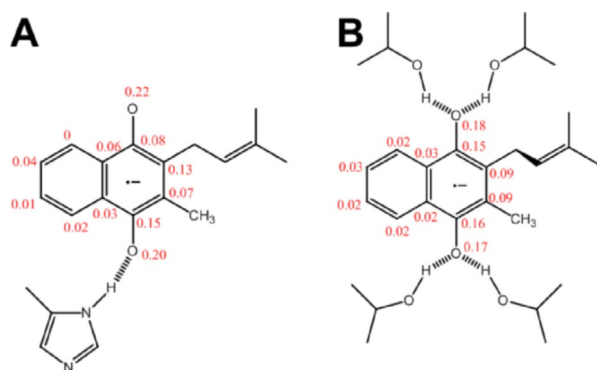


Figure 6. Comparison of calculated Mulliken spin populations on the ring carbon and oxygen atoms in MSK (with truncated isoprenyl chain) in different environments: (A) Im-MSK model 6; (B) IP₄-MSK model. Hydrogen bonds are indicated by dashed lines. An alternative representation is provided in Figure S4.

bond to the carbonyl oxygen O1, as compared with oxygen O4, leads to an increase of spin density on carbon 3 but a $\approx 33\%$ decrease of the spin density on carbon 2, which carries the methyl group. This value is in close agreement with the $\approx 29\%$ decrease that was estimated in our previous work by using the McConnell relation and the experimental $A_{\text{iso}}(^1\text{H}_{\text{Me}})$ values for MSK_D and for the corresponding radical measured in 2-propanol.^[23,39,65] Overall, despite the simple model of the MSK_D binding mode given by the Im-MSK model 6, the good agreement between the DFT calculated and the experimentally determined hyperfine and quadrupolar parameters shown in Table 3 supports a one-sided binding mode for MSK_D.

The few protein-bound SQ intermediates characterized in detail so far exhibit a variable distribution of the electron spin density over the aromatic ring. This distribution ranges from the very high asymmetry in the Q_A site of type II photosynthetic reaction centers, in the phylloquinone A₁ site of photosystem I or in the high affinity Q_H site in cytochrome *bo*₃, to a more symmetric spin density as measured in the Q_B site of type II photosynthetic reaction centers or for SQs in protic solvents.^[10,11,29,66] This observation has been discussed with regard to the quinone electron transfer role as one-electron (Q_A, A₁, and Q_H) or two-electron transfer agent (Q_B, quinones in vitro) coupled to the binding or release of two protons.^[44] Whereas the number of studied systems is too low for substantial conclusions, the present study provides an unprecedented example of a quinone with an extremely high asymmetric spin density distribution for the MSK_D intermediate whereas menaquinols in the Q_D site are in dynamic equilibrium with the quinone pool and bind to release two electrons and two protons before unbinding in the oxidized menaquinone form. It can therefore be concluded that the production within a Q site of a highly asymmetric spin density distribution for the SQ intermediate does not systematically translate into a role as a one-electron transfer agent for this Q site.

Interestingly, the asymmetry in the spin density distribution for the SQ reflects a more localized electron density distribution for the singly occupied molecular orbital of the free radical anion. Although this distribution would be expected to

lead to a less stable SQ form compared with the symmetrical form, the SQ stability constant measured by EPR-monitored redox titrations at equilibrium has been shown to be particularly high in the NarGHI Q_D site^[62] or in the cytochrome *bo*₃ Q_H site^[67,68] in comparison with other respiratory enzymes. Clearly, further investigations are necessary to assess the functional relevance of the different SQ redox and electronic properties measured in the investigated protein Q sites.

3. Conclusions

HYSCORE measurements performed on NarGHI samples prepared by using *in vivo* selective enrichment strategies in ²H or ¹⁵N nuclei provide direct evidence for the binding of MSK_D to a His N δ assigned to the heme *b*_D axial ligand His66. In addition, our results are consistent with a through-space interaction between the Lys86 N ζ and the radical. Finally, the isotropic hyperfine coupling constant of the freely rotating methyl protons is unambiguously determined from the measurement of the corresponding parameter on the semiquinone intermediate with selective deuteration of the menaquinone methyl group. It has the lowest value measured so far for methyl protons of vitamin K molecules (i.e., menadione, menaquinones, and phyloquinones) bound to proteins or dissolved in protic solvents. DFT calculations were performed by using a simple model of the Q_D site consisting of a menaquinone anion hydrogen bonded to an imidazole ring. Calculated EPR parameters are in good agreement with the available experimental data on MSK_D, showing that the presence of a single short hydrogen bond can fully account for the asymmetry of the spin density distribution in the radical anion MSK_D^{•-} inferred from our work. Further investigations are necessary to understand the functional significance of the extremely asymmetric binding mode of MSK_D.

Experimental Section

Bacterial Strains, Plasmids, and Growth Conditions

The *E. coli* strains and plasmids used in this study are described in Table 4. *E. coli* strains were routinely grown aerobically in lysogeny broth (LB) lennox medium at 37 °C supplemented with antibiotics when necessary. Auxotrophic strains were constructed by inactivation of selected genes with a kanamycin resistance cassette. The *metA*, *hisG*, and *lysA* genes were inactivated by replacement in the nitrate reductase-deficient JCB4023 strain^[69] by using Bacteriophage P1 transduction^[70] from the JW3973, JW2001, and JW2806 strains of the Keio collection, respectively.^[71] Each transductant strain was selected in LB broth lennox medium supplemented with casaminoacids (0.05%) and containing kanamycin (30 $\mu\text{g mL}^{-1}$) and spectinomycin (25 $\mu\text{g mL}^{-1}$). Deletion of the *metA*, *hisG*, and *lysA* genes was verified by the Met, His, and Lys auxotrophic phenotypes, respectively.

The Met auxotrophic LCB3766 strain was used for selective ²H-labeling at the methyl groups of endogenous menaquinones, whereas the LCB3514 and LCB3515 strains were used for selective ¹⁵N-labeling of Lysine and Histidine aminoacids, respectively. Notably, ²H-labeling of methyl groups belonging to the isoprenoid side chain likely occurs as well.^[41,74]

Table 4. *E. coli* strains and plasmid used in this study.

Strains/plasmids	Description	Reference/Source
<i>E. coli</i> strains		
JCB4023	RK4353 <i>narG:ery ΔnapA-B,narZ:Ω</i> , <i>spcR</i>	[70]
BW25113	<i>lacI q rrmB T14 ΔlacZ WJ16 hsdR514 ΔaraBAD AH33 ΔrhaBAD LD78</i>	[73]
JW2001	BW25113 <i>ΔhisG788:kan</i>	[72]
JW2806	BW25113 <i>ΔlysA763:kan</i>	[72]
JW3973	BW25113 <i>ΔmetA780:kan</i>	[72]
LCB3514	RK4353 <i>narG:ery ΔnapA-B,narZ:Ω ΔlysA763:kan</i>	this work
LCB3515	RK4353 <i>narG:ery ΔnapA-B,narZ:Ω ΔhisG788:kan</i>	this work
LCB3766	RK4353 <i>narG:ery ΔnapA-B,narZ:Ω ΔmetA780:kan</i>	this work
Plasmid		
pVA700	pJF119EH <i>narGHJI</i> , <i>ampR</i>	[74]
[*] Resistance cassettes: <i>spcR</i> : spectinomycin, <i>kan</i> : kanamycin, <i>ampR</i> : ampicillin.		

For NarGHI overproduction, the strains were transformed with the pVA700 plasmid and grown semi-aerobically at 37 °C in defined minimal medium^[51] supplemented by either [methyl-²H] methionine (35 μM, isotope purity 98%, Cambridge Isotope Laboratories, Inc), L-lysine-ε-¹⁵N-2HCl (136 μM, isotope purity 98%, euriso-top), or L-histidine-δ-¹⁵N-HCl·H₂O (142 μM; isotope purity 98%, euriso-top) and by 0.2 mM of isopropyl 1-thio-β-D-galactopyranoside to induce the *narGHJI* expression. Typically, cells were first grown aerobically at 37 °C until stationary phase in 60 mL LB medium supplemented with casaminoacids (0.05%) and containing kanamycin (30 μg mL⁻¹), spectinomycin (25 μg mL⁻¹), and ampicillin (100 μg mL⁻¹). Then, cells were used to inoculate (starting optical density (OD) ≈ 0.1) a 500 mL overnight semi-anaerobic preculture by using the above-mentioned defined minimal medium^[51] with kanamycin (15 μg mL⁻¹) and ampicillin (50 μg mL⁻¹). The preculture was harvested by centrifugation, washed twice with minimal medium, and resuspended to an OD ≈ 0.1 in 2.5 L of fresh minimal medium supplemented with the desired labeled amino acid and ampicillin (50 μg mL⁻¹).

Preparation of Membrane Fractions and of Selectively Labeled Samples

Purified *E. coli* NarGHI-enriched inner membrane vesicles (IMVs) were prepared as described previously elsewhere,^[46] by using a buffer containing 100 mM MOPS (3-(*N*-morpholino)propanesulfonic acid) and 5 mM EDTA (ethylenediaminetetraacetic acid) at pH 7.5 or pH 8.5, frozen in liquid N₂, and stored at -80 °C until use. The NarGHI concentration in IMVs was estimated by the rocket immunoelectrophoresis method.^[75,76] The nitrate reductase concentration was ≈ 170 μM in the L-lysine-ε-¹⁵N-2HCl sample, and ≈ 210 μM for the L-histidine-δ-¹⁵N-HCl·H₂O sample. Stabilization of MSK_D was achieved through redox titrations under the same conditions as those used in our previous work.^[62] Redox potentials are given in the text with respect to the standard hydrogen electrode.

EPR and HYSORE Measurements

X-band continuous wave (cw) EPR experiments were performed with a Bruker EleXsys E500 spectrometer equipped with an ER4102ST standard rectangular Bruker EPR cavity fitted to an Oxford Instruments helium flow cryostat. 2D HYSORE experiments were carried out on the same samples by using a Bruker EleXsys

E580 spectrometer equipped with an ER4118X-MD5 dielectric resonator and an Oxford Instruments CF 935 cryostat. This four-pulse experiment ($\pi/2-\tau-\pi/2-t_1-\pi-t_2-\pi/2-\tau$ -echo) was employed with appropriate phase-cycling schemes to eliminate unwanted features from the experimental electron spin echo envelopes. The intensity of the echo after the fourth pulse was measured with varied t_2 and t_1 and constant τ . HYSORE data were collected in the form of 2D time-domain patterns containing 256 × 256 points. They were recorded at 90 K and at the magnetic field value corresponding to the maximum intensity of the MSK signal measured in a two-pulse field sweep electron spin echo sequence ($\pi/2-\tau-\pi-\tau$ -echo).

HYSORE spectra were processed by using Bruker's Xepr software. Relaxation decays were subtracted (fitting by polynomial functions) followed by zero-filling and tapering with a Hamming window, before 2D Fourier transformation, which finally gives the spectrum in the frequency domain. Processed data were then imported into Matlab (The MathWorks Inc., Natick, MA) for plotting. HYSORE spectra are shown in absolute value mode and are presented as contour plots together with the skyline projection on the two frequency axes.

Spectral Simulations

Numerical simulations of HYSORE spectra were performed by using the EasySpin package (release 5.01.12) that works under Matlab (The MathWorks, Inc., US).^[77,78] For the simulation of HYSORE resonances given by quadrupolar nuclei, Euler angles, which describe the orientation of the P tensor with respect to the molecular frame (analogous to the g frame), were used. The A and g frames were assumed to be collinear.

DFT Calculations

All calculations have been performed with the Orca 3.0 quantum chemistry package^[79] at a DFT level of theory, by using the B3LYP hybrid functional (the Becke's three-parameter hybrid exchange functional with 20% Hartree-Fock admixture and the Lee-Yang-Parr non-local correlation functional). A restricted geometry optimization has been performed in vacuo on each model with the def2-SVP basis set.^[80,81] The resolution of identity with the appropriate auxiliary basis sets was used to accelerate the calculations.^[82] The optimized structures have then been used as input for electronic and magnetic properties calculations, by using the EPR-II basis set^[83] and employing the conductor-like screening model COSMO^[84] with a dielectric constant $\epsilon = 4.0$ to replicate the electrostatic effects of the protein surrounding. ¹H hyperfine and ²H nuclear quadrupole coupling constants of the methyl group were calculated by averaging the raw matrices corresponding to the three positions of the methyl protons and the eigenvalues and eigenvectors were determined.

Hyperfine and Nuclear Quadrupole Interactions

A hyperfine coupling between a SQ and a nucleus with nuclear spin value I consists in general of (i) an isotropic contribution $A_{\text{iso}} = 2\mu_0 g_e g_n \beta_e \beta_n |\psi_0(0)|^2 / 3h$ where $|\psi_0(0)|^2$ is the electron spin density at the nucleus, g_e and g_n are electron and nuclear g -factors, respectively, β_e and β_n are the Bohr and nuclear magneton, respectively, h is Planck's constant, and (ii) an anisotropic contribution described

by the dipolar coupling tensor \tilde{T} . The typical approach used for estimation of this contribution considers the dipole–dipole approximation between the nucleus and the unpaired spin density localized on the nearest carbonyl oxygen of the SQ. In this case, \tilde{T} has axial symmetry with principal values ($A_{\text{iso}} - T$, $A_{\text{iso}} - T$, $A_{\text{iso}} + 2T$) with T given in Equation (1) as:

$$T = \rho_0 g_e g_n \beta_e \beta_n / hr^3 = \rho_0 (b/r^3) \quad (1)$$

where r is the distance between the nucleus and the electron point dipole, ρ_0 is the π spin density at the quinone oxygen, $b = 12.14 \text{ MHz \AA}^3$ (for ^2H) and 8.02 MHz \AA^3 (for ^{15}N). The hyperfine couplings of different isotopes of the same element are proportional to a very good approximation to the corresponding g_n values.

^2H and ^{14}N nuclei have a quadrupole moment that interacts with the electric field gradient (EFG) at the nucleus. The components of the EFG tensor are defined in its principal axis system and are ordered according to $|q_{zz}| \geq |q_{yy}| \geq |q_{xx}|$. This traceless tensor can then be fully described by only two parameters: (i) the nuclear quadrupole coupling constant $\kappa = |e^2 q_{zz} Q / h|$, where e is the charge of an electron, Q is the nuclear electric quadrupole moment of the nucleus, (ii) the asymmetry parameter $\eta = |q_{yy} - q_{xx}| / q_{zz}$. κ is a measure of the strength of the interaction between the nuclear quadrupole moment and the EFG at the nucleus site owing to anisotropic charge distribution in the system whereas η is a measure of the deviation of the charge distribution from axial symmetry. κ and η are extremely sensitive to atomic and chemical bond arrangements and are excellent probes for the identification of bonding geometry and of the chemical group housing the nucleus.

Acknowledgments

This work has been supported by the French national research agency (ANR, ERMoE project, grant number ANR-06-PCVI-0003, <https://anrnc2.wordpress.com>), the CNRS "Mission pour l'Interdisciplinarité" program (project "Instrumentations aux limites"), the A*Midex foundation of Aix-Marseille University (project MicroBioE, grant number ANR-11-IDEX-0001-02) and the French EPR network (RENARD, IR3443, <http://renard.univ-lille1.fr>). S.G. acknowledges the Research Infrastructures Activity in the 6th Framework Program of the European Union (Contract RII3-026145, EU-NMR) for funding Short-Term Scientific Missions. Prof. T. F. Prisner (University of Frankfurt, Germany) is gratefully acknowledged for granting access to his instrumentation that was used for part of this work. DFT calculations were performed by using computing resources from the "Centre Régional de Compétences en Modélisation Moléculaire" (CRCMM; Marseille). We thank G. Gerbaud and E. Etienne for maintenance of the EPR facility in Marseille. M.S.E. and J.R. were supported by Ph.D. fellowships from the Lebanese Government and from the CNRS/Région Provence-Alpes-Côte d'Azur, respectively.

Conflict of interest

The authors declare no conflict of interest.

Keywords: bioenergetics • electron transfer • EPR spectroscopy • metalloenzymes • quinones

- [1] B. Nowicka, J. Kruk, *Biochim. Biophys. Acta Bioenerg.* **2010**, 1797, 1587–1605.
- [2] M. D. Collins, D. Jones, *Microbiol. Rev.* **1981**, 45, 316–354.
- [3] B. Schoepp-Cothenet, R. van Lis, A. Atteia, F. Baymann, L. Capowiez, A. L. Ducluzeau, S. Duval, F. T. Brink, M. J. Russell, W. Nitschke, *Biochim. Biophys. Acta Bioenerg.* **2013**, 1827, 79–93.
- [4] E. Maklashina, G. Cecchini, S. A. Dikanov, *Biochim. Biophys. Acta Bioenerg.* **2013**, 1827, 668–678.
- [5] N. Srinivasan, J. H. Golbeck, *Biochim. Biophys. Acta Bioenerg.* **2009**, 1787, 1057–1088.
- [6] J. L. Cape, M. K. Bowman, D. M. Kramer, *Trends Plant Sci.* **2006**, 11, 46–55.
- [7] R. Pietras, M. Sarewicz, A. Osyczka, *J. R. Soc. Interface* **2016**, 13, 20160133.
- [8] J. Hirst, M. M. Roessler, *Biochim. Biophys. Acta Bioenerg.* **2016**, 1857, 872–883.
- [9] P. K. Singh, M. Sarwar, E. Maklashina, V. Kotlyar, S. Rajagukguk, T. M. Tomasiak, G. Cecchini, T. M. Iverson, *J. Biol. Chem.* **2013**, 288, 24293–24301.
- [10] S. A. Dikanov in *Resolving Protein–Semiquinone Interactions by Two-Dimensional ESEEM Spectroscopy*, Vol. 23, The Royal Society of Chemistry, London, **2013**, pp. 103–179.
- [11] W. Lubitz, G. Feher, *Appl. Magn. Reson.* **1999**, 17, 1–48.
- [12] M. Flores, R. Isaacson, E. Abresch, R. Calvo, W. Lubitz, G. Feher, *Biophys. J.* **2007**, 92, 671–682.
- [13] A. T. Taguchi, P. J. O'Malley, C. A. Wraight, S. A. Dikanov, *J. Phys. Chem. B* **2015**, 119, 5805–5814.
- [14] C. Sun, A. T. Taguchi, J. V. Vermaas, N. J. Beal, P. J. O'Malley, E. Tajklorshid, R. B. Gennis, S. A. Dikanov, *Biochemistry* **2016**, 55, 5714–5725.
- [15] F. MacMillan, S. Kacprzak, P. Hellwig, S. Grimaldi, H. Michel, M. Kaupp, *Faraday Discuss.* **2011**, 148, 315–344.
- [16] S. M. Yi, K. V. Narasimhulu, R. I. Samoilova, R. B. Gennis, S. A. Dikanov, *J. Biol. Chem.* **2010**, 285, 18241–18251.
- [17] S. A. Dikanov, J. T. Holland, B. Endeward, D. R. Kolling, R. I. Samoilova, T. F. Prisner, A. R. Crofts, *J. Biol. Chem.* **2007**, 282, 25831–25841.
- [18] S. Grimaldi, R. A. Cartin, P. Lanciano, S. Lyubenova, B. Endeward, T. F. Prisner, A. Magalon, B. Guigliarelli, *J. Biol. Chem.* **2010**, 285, 179–187.
- [19] E. Martin, R. I. Samoilova, K. V. Narasimhulu, C. A. Wraight, S. A. Dikanov, *J. Am. Chem. Soc.* **2010**, 132, 11671–11677.
- [20] J. Hanley, Y. Deligiannakis, F. MacMillan, H. Bottin, A. W. Rutherford, *Biochemistry* **1997**, 36, 11543–11549.
- [21] J. M. Pelloquin, X. S. Tang, B. A. Diner, R. D. Britt, *Biochemistry* **1999**, 38, 2057–2067.
- [22] Y. Deligiannakis, A. Boussac, A. W. Rutherford, *Biochemistry* **1995**, 34, 16030–16038.
- [23] S. Grimaldi, R. Arias-Cartin, P. Lanciano, S. Lyubenova, R. Szenes, B. Endeward, T. F. Prisner, B. Guigliarelli, A. Magalon, *J. Biol. Chem.* **2012**, 287, 4662–4670.
- [24] S. A. Dikanov, R. I. Samoilova, D. R. Kolling, J. T. Holland, A. R. Crofts, *J. Biol. Chem.* **2004**, 279, 15814–15823.
- [25] H. Dobbek, *Coord. Chem. Rev.* **2011**, 255, 1104–1116.
- [26] M. Flores, R. Isaacson, E. Abresch, R. Calvo, W. Lubitz, G. Feher, *Biophys. J.* **2006**, 90, 3356–3362.
- [27] A. V. Veselov, J. P. Osborne, R. B. Gennis, C. P. Scholes, *Biochemistry* **2000**, 39, 3169–3175.
- [28] I. P. Muhiuddin, S. E. Rigby, M. C. Evans, J. Amesz, P. Heathcote, *Biochemistry* **1999**, 38, 7159–7167.
- [29] J. Niklas, B. Epel, M. L. Antonkine, S. Sinnecker, M. E. Pandelia, W. Lubitz, *J. Phys. Chem. B* **2009**, 113, 10367–10379.
- [30] S. Kacprzak, M. Kaupp, F. MacMillan, *J. Am. Chem. Soc.* **2006**, 128, 5659–5671.
- [31] E. Martin, R. I. Samoilova, K. V. Narasimhulu, T. J. Lin, P. J. O'Malley, C. A. Wraight, S. A. Dikanov, *J. Am. Chem. Soc.* **2011**, 133, 5525–5537.
- [32] S. Sinnecker, M. Flores, W. Lubitz, *Phys. Chem. Chem. Phys.* **2006**, 8, 5659–5670.
- [33] J. Fritscher, T. F. Prisner, F. MacMillan, *Appl. Magn. Reson.* **2006**, 30, 251–268.

- [34] C. Teutloff, R. Bittl, W. Lubitz, *Appl. Magn. Reson.* **2004**, *26*, 5–21.
- [35] B. Epel, J. Niklas, S. Sinnecker, H. Zimmermann, W. Lubitz, *J. Phys. Chem. B* **2006**, *110*, 11549–11560.
- [36] S. Sinnecker, E. Reijerse, F. Neese, W. Lubitz, *J. Am. Chem. Soc.* **2004**, *126*, 3280–3290.
- [37] A. M. Weyers, R. Chatterjee, S. Milikisiyants, K. V. Lakshmi, *J. Phys. Chem. B* **2009**, *113*, 15409–15418.
- [38] F. MacMillan, F. Lendzian, W. Lubitz, *Magn. Reson. Chem.* **1995**, *33*, S81–S93.
- [39] A. T. Gardiner, S. G. Zech, F. MacMillan, H. Kass, R. Bittl, E. Schlodder, F. Lendzian, W. Lubitz, *Biochemistry* **1999**, *38*, 11773–11787.
- [40] M. T. Lin, L. J. Sperling, H. L. F. Schmidt, M. Tang, R. I. Samoilova, T. Kumazaka, T. Iwasaki, S. A. Dikanov, C. M. Rienstra, R. B. Gennis, *Methods* **2011**, *55*, 370–378.
- [41] P. Heathcote, P. Moenne-Loccoz, S. E. Rigby, M. C. Evans, *Biochemistry* **1996**, *35*, 6644–6650.
- [42] S. E. Rigby, M. C. Evans, P. Heathcote, *Biochemistry* **1996**, *35*, 6651–6656.
- [43] M. T. Lin, R. I. Samoilova, R. B. Gennis, S. A. Dikanov, *J. Am. Chem. Soc.* **2008**, *130*, 15768–15769.
- [44] M. T. Lin, A. Baldansuren, R. Hart, R. I. Samoilova, K. V. Narasimhulu, L. L. Yap, S. K. Choi, P. J. O'Malley, R. B. Gennis, S. A. Dikanov, *Biochemistry* **2012**, *51*, 3827–3838.
- [45] M. G. Bertero, R. A. Rothery, N. Boroumand, M. Palak, F. Blasco, N. Ginot, J. H. Weiner, N. C. Strynadka, *J. Biol. Chem.* **2005**, *280*, 14836–14843.
- [46] P. Lanciano, A. Magalon, P. Bertrand, B. Guigliarelli, S. Grimaldi, *Biochemistry* **2007**, *46*, 5323–5329.
- [47] F. Blasco, B. Guigliarelli, A. Magalon, M. Asso, G. Giordano, R. A. Rothery, *Cell. Mol. Life Sci.* **2001**, *58*, 179–193.
- [48] M. G. Bertero, R. A. Rothery, M. Palak, C. Hou, D. Lim, F. Blasco, J. H. Weiner, N. C. Strynadka, *Nat. Struct. Biol.* **2003**, *10*, 681–687.
- [49] S. Grimaldi, B. Schoepp-Cothenet, P. Ceccaldi, B. Guigliarelli, A. Magalon, *Biochim. Biophys. Acta Bioenerg.* **2013**, *1827*, 1048–1085.
- [50] R. Arias-Cartin, S. Lyubenova, P. Ceccaldi, T. Prisner, A. Magalon, B. Guigliarelli, S. Grimaldi, *J. Am. Chem. Soc.* **2010**, *132*, 5942–5943.
- [51] J. Rendon, E. Pilet, Z. Fahs, F. Seduk, L. Sylvi, M. H. Chehade, F. Pierrel, B. Guigliarelli, A. Magalon, S. Grimaldi, *Biochim. Biophys. Acta Bioenerg.* **2015**, *1847*, 739–747.
- [52] M. T. Lin, A. A. Shubin, R. I. Samoilova, K. V. Narasimhulu, A. Baldansuren, R. B. Gennis, S. A. Dikanov, *J. Biol. Chem.* **2011**, *286*, 10105–10114.
- [53] S. J. Hong, W. B. de Almeida, A. T. Taguchi, R. I. Samoilova, R. B. Gennis, P. J. O'Malley, S. A. Dikanov, A. R. Crofts, *Biochemistry* **2014**, *53*, 6022–6031.
- [54] P. J. O'Malley, *J. Phys. Chem. A* **1998**, *102*, 248–253.
- [55] P. J. O'Malley, *Biochim. Biophys. Acta Bioenerg.* **1999**, *1411*, 101–113.
- [56] M. Kaupp, C. Remenyi, J. Vaara, O. L. Malkina, V. G. Malkin, *J. Am. Chem. Soc.* **2002**, *124*, 2709–2722.
- [57] J. R. Asher, N. L. Doltsinis, M. Kaupp, *J. Am. Chem. Soc.* **2004**, *126*, 9854–9861.
- [58] J. Fritscher, *Phys. Chem. Chem. Phys.* **2004**, *6*, 4950–4956.
- [59] J. R. Asher, N. L. Doltsinis, M. Kaupp, *Magn. Reson. Chem.* **2005**, *43*, S237–S247.
- [60] F. Himo, G. T. Babcock, L. A. Eriksson, *J. Phys. Chem. A* **1999**, *103*, 3745–3749.
- [61] M. Zheng, G. C. Dismukes, *Biochemistry* **1996**, *35*, 8955–8963.
- [62] S. Grimaldi, P. Lanciano, P. Bertrand, F. Blasco, B. Guigliarelli, *Biochemistry* **2005**, *44*, 1300–1308.
- [63] M. R. Das, H. D. Connor, D. S. Leniart, J. H. Freed, *J. Am. Chem. Soc.* **1970**, *92*, 2258–2268.
- [64] S. F. Hastings, P. Heathcote, W. J. Ingledew, S. E. Rigby, *Eur. J. Biochem.* **2000**, *267*, 5638–5645.
- [65] H. M. McConnell, *J. Chem. Phys.* **1956**, *24*, 764–766.
- [66] S. Grimaldi, T. Ostermann, N. Weiden, T. Mogi, H. Miyoshi, B. Ludwig, H. Michel, T. F. Prisner, F. MacMillan, *Biochemistry* **2003**, *42*, 5632–5639.
- [67] M. Sato-Watanabe, S. Itoh, T. Mogi, K. Matsuura, H. Miyoshi, Y. Anraku, *FEBS Lett.* **1995**, *374*, 265–269.
- [68] W. J. Ingledew, T. Ohnishi, J. C. Salerno, *Eur. J. Biochem.* **1995**, *227*, 903–908.
- [69] L. C. Potter, J. A. Cole, *Biochem. J.* **1999**, *344*, 69–76.
- [70] L. C. Thomason, N. Costantino, D. L. Court, *E. coli Genome Manipulation by P1 Transduction*, in *Curr. Protoc. Mol. Bio.* **2007**, 1.17.11–11.17.18.
- [71] T. Baba, T. Ara, M. Hasegawa, Y. Takai, Y. Okumura, M. Baba, K. A. Datsenko, M. Tomita, B. L. Wanner, H. Mori, *Mol. Syst. Biol.* **2006**, *2*, 2006.0008.
- [72] K. A. Datsenko, B. L. Wanner, *Proc. Natl. Acad. Sci. USA* **2000**, *97*, 6640–6645.
- [73] B. Guigliarelli, A. Magalon, M. Asso, P. Bertrand, C. Frixon, G. Giordano, F. Blasco, *Biochemistry* **1996**, *35*, 4828–4836.
- [74] B. A. Barry, C. J. Bender, L. McIntosh, S. Fergusonmiller, G. T. Babcock, *Isr. J. Chem.* **1988**, *28*, 129–132.
- [75] V. Augier, M. Asso, B. Guigliarelli, C. More, P. Bertrand, C. L. Santini, F. Blasco, M. Chippaux, G. Giordano, *Biochemistry* **1993**, *32*, 5099–5108.
- [76] V. Augier, B. Guigliarelli, M. Asso, P. Bertrand, C. Frixon, G. Giordano, M. Chippaux, F. Blasco, *Biochemistry* **1993**, *32*, 2013–2023.
- [77] S. Stoll, R. D. Britt, *Phys. Chem. Chem. Phys.* **2009**, *11*, 6614–6625.
- [78] S. Stoll, A. Schweiger, *J. Magn. Reson.* **2006**, *178*, 42–55.
- [79] F. Neese, *Wiley Interdisciplinary Rev.: Comput. Mol. Sci.* **2012**, *2*, 73–78.
- [80] A. Schäfer, H. Horn, R. Ahlrichs, *J. Chem. Phys.* **1992**, *97*, 2571–2577.
- [81] A. Schäfer, C. Huber, R. Ahlrichs, *J. Chem. Phys.* **1994**, *100*, 5829–5835.
- [82] F. Neese, *J. Comput. Chem.* **2003**, *24*, 1740–1747.
- [83] V. Barone, *Structure, Magnetic Properties and Reactivities of Open-Shell Species from Density Functional and Self-Consistent Hybrid Methods*, in *Recent Advances in Density Functional Methods* (Ed.: D. P. Chong), World Scientific, Singapore, **1995**, pp. 287–334.
- [84] A. Klamt, G. Schuurmann, *J. Chem. Soc. Perkin Trans. 2* **1993**, 799–805.

Manuscript received: May 24, 2017

Revised manuscript received: July 4, 2017

Accepted manuscript online: July 6, 2017

Version of record online: August 28, 2017